ADVANCED OPTICAL MATERIALS
www.advopticalmat.de

www.MaterialsViews.com

Distributing the Optical Near-Field for Efficient Field-Enhancements in Nanostructures

V. K. Valev, B. De Clercq, C. G. Biris, X. Zheng, S. Vandendriessche, M. Hojeij, D. Denkova, Y. Jeyaram, N. C. Panoiu, Y. Ekinci, A. V. Silhanek, V. Volskiy, G. A. E. Vandenbosch, M. Ameloot, V. V. Moshchalkov, and T. Verbiest*

When molecules approach a nanostructured metal surface that is illuminated by visible light, these molecules experience a very intricate electric field. On the one hand, the field results from light itself, which is incident on the nanostructures, scattered and diffracted from them or reflected from their interfaces. On the other hand, light's electromagnetic oscillations drive the electron density within the nanostructures and, in turn, these variations of electron density constitute the source of a very inhomogeneous surface electric field–the local field.[1] Molecules placed in the local field experience electric forces along the field lines, which become very crowded in two sorts of regions on the nanostructures. First, in the sharp regions, such as corners or tips, where the field lines are pulled together by geometric constraints. And second, in the regions of highest electron density, where the electron charges constitute strong sources for the local field. These regions of crowded field lines, at the nanostructured metal surface, correspond to local field enhancements and are commonly referred to as "hotspots". One of the reasons why such hotspots are very important, is because of what can happen to molecules within them.

Within hotspots, molecules can experience chemical transformations,[2] photochemical reactions,[3] catalytic reactions[4,5] and extreme enlargement of their optical properties.[6,7] A particularly spectacular example is surface enhanced Raman scattering,[8] whereby the Raman signal can be increased up to fourteen orders of magnitude.[9,10] Unfortunately though, hotspots suffer from two limiting factors–they can become too hot and they are only spots.

Indeed, in an attempt to achieve ever greater enlargement of the optical response of molecules, the incident light intensity can be increased. Besides the desired increase of the local field intensity however, an undesired increase of nanostructure heating occurs. The heating is due to the local electric currents that are associated with the oscillations of the electron density, according to Joule's effect. It has thus been shown that, in the hotspots, laser-induced heating can melt the nanostructures and even give rise to hydrodynamic processes.[11,12] Therefore, there is an upper limit to how much the local field can be enhanced within a hotspot without inducing irreversible damage to the surface of the sample. In order to further benefit from enlarged optical response of molecules, a better choice might be to nanoengineer *larger* spots.

Recently, there has been considerable efforts towards engineering local field enhancements. Hotspots can thus be obtained at randomly roughened surfaces,[13,14] through plasmon excitations,[15] due to nanostructuring,[16] or by making use of antenna designs.[17] In all of these cases, local field enhancement occurs only within a small region of the sample surface. From a practical point of view, it would be very interesting to expand the local field enhancements to the whole sample surface, thereby increasing the opportunity for interaction with molecules. Because it originates from the inhomogeneity of electron density in the nanostructures, such an expanded field can still be called "local" in nature, however it would no longer be *localized* in small spots. To avoid any confusion, from now on, we shall designate this field as the "near-field". As we shall prove in this work, an effective approach to obtain near-field enhancements over the entire sample surface is to drive the electron surface currents along ring-shaped nanostructures.

Dr. V. K. Valev,[+] S. Vandendriessche, Prof. T. Verbiest
Molecular Electronics and Photonics
INPAC, Katholieke Universiteit Leuven
BE-3001, Belgium
E-mail: v.k.valev@fys.kuleuven.be

B. De Clercq, Prof. M. Ameloot
University Hasselt and transnational University Limburg
BIOMED, Diepenbeek, Belgium

Dr. C. G. Biris, Dr. N. C. Panoiu
Department of Electronic and Electrical Engineering
University College London
Torrington Place, London, WC1E 7JE, UK

X. Zheng, Dr. V. Volskiy, Prof. G. A. E. Vandenbosch
SAT-TELEMIC, Katholieke Universiteit Leuven
B-3001 Leuven, Belgium

M. Hojeij
Paul Scherrer Institute
5232 Villigen-PSI, Switzerland

Dr. Y. Ekinci
Laboratory for Micro and Nanotechnology
Paul Scherrer Institute
5232 Villigen-PS, Switzerland and Laboratory
of Metal Physics and Technology
Department of Materials
ETH Zurich, 8093 Zurich, Switzerland

D. Denkova, Y. Jeyaram, Prof. V. V. Moshchalkov
Superconductivity and Magnetism & Pulsed Fields Group
INPAC, Katholieke Universiteit Leuven
BE-3001, Belgium

Prof. A. V. Silhanek
Département de Physique
Université de Liège
Bât. B5, Allée du 6 août, 17, Sart Tilman, B-4000, Belgium

[+] Present Address: Dipartimento di Scienze di Base ed Applicate per l'Ingegneria – Sapienza Università di Roma, Via A. Scarpa 14, I-00161 Roma, Italy

DOI: 10.1002/adma.201201151

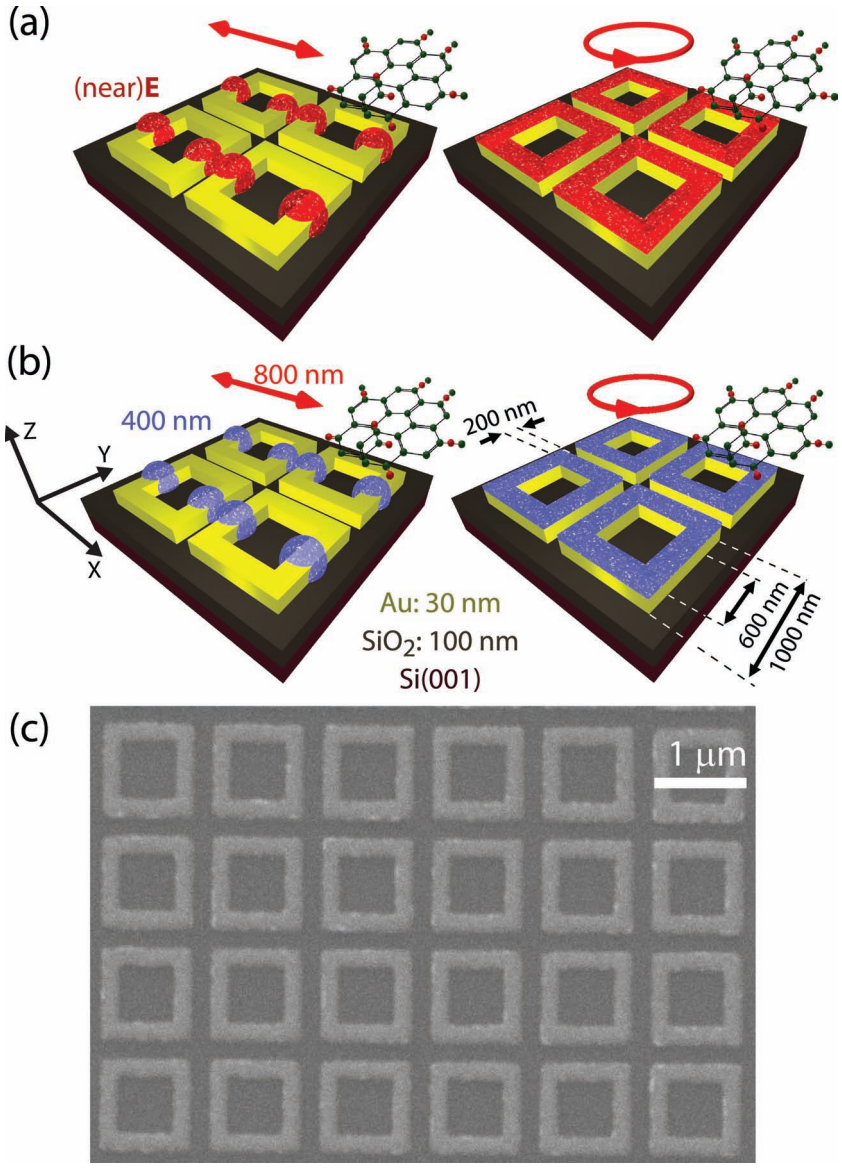

Figure 1. Increasing the interaction cross-section between molecules and enhanced optical near-field in nanostructures. In (a), in response to linearly polarized incident light (red arrow), local field enhancements of the electric field form hotspots on the surface of square-ring gold nanostructures. For circularly polarized incident light (red oriented circle), the electric local field enhancements are homogeneous on the entire surface of the nanostructures. In (b), the second harmonic generation matches the pattern of electric local field enhancements for both linearly and circularly polarized light. In (c), scanning electron microscopy image of the fabricated gold nanostructures.

Here we demonstrate that circularly polarized light imparts a sense of rotation on the electron density in ring-shaped gold nanostructures. As a consequence, the near-field enhancement becomes homogeneous on the surface of the nanostructures, thereby increasing the opportunity for interaction with molecules, see **Figures 1**a and 1b. Interestingly, for linearly polarized light oriented along the Y and X directions, a pattern of pronounced hotspots indicates strong coupling between the nanostructures along these directions. Upon rotating the direction of linearly polarized light, the pattern of hotspots does not always follow the direction of polarization but instead appears "pinned" by the strong coupling along the Y and X directions. Consequently, while for circularly polarized light the near-field is *homogeneous*, for randomly distributed linearly polarized light the near-field is *inhomogeneous*. This difference reflects the difference in electron density behavior, depending on the nature of light polarization. The work presented here is intended as a proof of principle; by varying the dimensions and the shape of the metallic rings, further device optimization can be obtained. As a guideline for such device optimization, we propose a quantitative figure or merit for homogeneity of surface near-fields. This type of nanostructured samples can find a broad range of applications in chemical processes where the interaction between molecules and local field enhancements play an important role. In order to maximize the useful sample surface, we avoided using circular rings, which do not pack very efficiently, and instead preferred square-rings.

The square-ring shaped nanostructures are made of gold (30 nm thick) grown on top of SiO_2 (100 nm)/Si(001) substrate, and are produced by electron beam lithography. More details on the deposition and on the rest of the sample preparation can be found in Ref. 18. The outer side of each square measures 1000 nm, the width of the metallic stripes is 200 nm, and all the nanostructures are 200 nm apart from each other, as shown in Figure 1c. The total area of the sample is 2.5 by 2.5 mm. When these structures are illuminated at the wavelength of 800 nm, a plasmon resonance is excited. The presence of the resonance was evidenced by numerically simulating the reflection and transmission spectra of the nanostructures, see **Figure 2**a. Moreover, for the purpose of completeness, the same nanostructures were deposited on a transparent substrate (glass), so that reflection and transmission spectra could also be experimentally verified, see Figure 2b. It should be noted that the small difference between the experimentally and computationally determined spectra is due to the fact that we did not include the substrate in the numerical simulations. As Figure 2 illustrates, this difference increases with the wavelength due to the frequency dispersion of both the index of refraction and of the absorption coefficient of the substrate. Despite the small difference in peak positions, the numerical simulation are in excellent agreement with the experimental measurements. At resonance, reflection from different interfaces, scattering, diffraction and various near-field enhancements can be observed. All of these phenomena are rigorously taken into account in numerical solvers of Maxwell equations, which are therefore suitable for mapping with high resolution the electromagnetic fields.

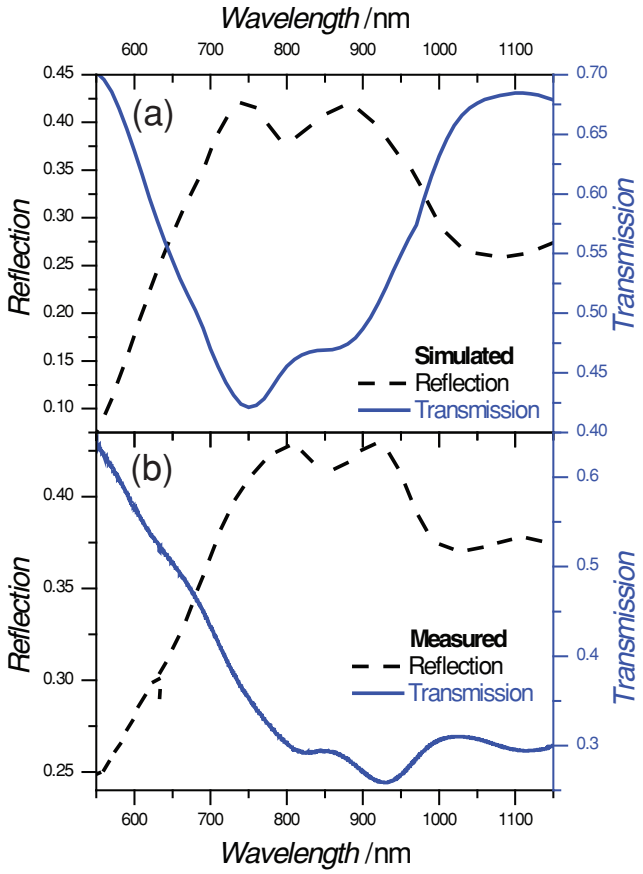

Figure 2. For linearly polarized incident light, reflection and transmission spectra from the square-shaped gold nanostructures were numerically simulated and experimentally measured as is it shown in (a) and (b), respectively.

In order to accurately map the near-field enhancements at the surface of the gold nanostructures, we perform two independent numerical simulations. The first one, performed with RSoft's DiffractMOD,[19] evaluates the electric fields in air, 1 nm above the gold surface. The second one, performed with MAGMAS,[20,21] evaluates the electric currents inside the gold layer, 1 nm below the surface. Both simulations assume monochromatic wave excitation under normal incidence (the wavelength of the incoming light is 800 nm) and periodic boundary conditions, which significantly reduces the simulation time. **Figures 3**a and 3b show the electric field intensity for vertically and horizontally polarized light, respectively. In both cases, intense hotspots can be observed, corresponding to near-field enhancements on the opposing sides of the square-rings that are perpendicular to the direction of polarization. Because, in the case of circularly polarized light, both vertical and horizontal field components are present in equal amplitudes (yet out-of-phase by $\pi/2$), one might initially expect circularly polarized light to simply produce a superposition of the field profiles in Figure 3a and 3b, i.e. four hotspots, one on each side of the square-rings. Figures 3c and 3d show, however, that this is not the case. Our result indicates that the phase between the vertical and horizontal field components of circularly polarized light plays a crucial role in the generation of the near-field.

Indeed, for circularly polarized light, Figure 3c and 3d demonstrate that instead of exhibiting hotspots, the electric field intensities are spatially much more homogeneously distributed than in Figures 3a and 3b. A more careful examination of Figure 3c reveals that the near-field enhancement pattern has a sense of rotation that is mirrored in Figure 3d, even though the nanostructures are clearly not chiral. Consequently, it is the chirality of light that is imparted onto the near-fields of the nanostructures. In order to better understand this physical mechanism, we can examine the distribution of the electric currents, which are induced by light at the surface of the nanostructures.

Upon examining the distribution of electric currents at 1 nm below the surface of the nanostructures, the similarities with the electric near-fields become obvious. First, for linearly polarized light, there are hotspots on the square-ring sides that are perpendicular to the direction of polarization, see Figures 3e and 3f. And second, for circularly polarized light, there is a sense of rotation in the pattern, which can be related to the direction of circularly polarized light. Henceforth, Figure 3 clearly illustrates the agreement between two complementary theoretical approaches. This is a strong indication for the validity of the results, however for the sake of scientific rigor, an experimental confirmation is necessary. The experimental study is performed with second harmonic generation (SHG) microscopy, a technique whose usefulness for visualizing field enhancements in nanostructures has been demonstrated in several works already.[22–27] We use ultrafast pulsed lasers (~100 fs, 82 MHz), which are capable of delivering very high electric field intensities to the electron population in the nanostructures. When the intense electric field of light becomes comparable with the electric near-fields, the oscillations of the electron density are driven in the nonlinear (anharmonic) regime. This nonlinear regime can be described by a mathematical expansion in series, corresponding to higher order frequency terms. The second harmonic generation technique consists in measuring the term in the nonlinear expansion series that is associated with the double frequency of the illumination. An intuitively very appealing explanation for this technique is to consider that, in response to the electric field of light, most electrons within the nanostructures are driven in the linear regime. However, in the hotspots, due to near-field enhancements, the electrons are driven in the nonlinear regime. As a consequence, second harmonic signal is generated precisely from the regions of near-field enhancements. In essence, the technique offers built-in light sources for the near-field enhancement signal, at a frequency that is easily separable from any noise at the illumination frequency, such as scattering, diffraction or reflection. Therefore, SHG microscopy can accurately map near-field enhancements in nanostructures, see **Figure 4**.

Figure 4a, presents a SHG micrograph from the top left corner of the nanostructure array, for incident light linearly polarized along the vertical direction, as indicated by the white arrow. An array of hotspots can be observed. Most of them occur in pairs, which are oriented along the direction of polarization. Upon superimposing the layout of the nanostructures on the SHG micrograph, it becomes clear that the location of these hotspots corresponds to the sides of the square-ring nanostructures, which are perpendicular to the polarization. The same trend can be observed for horizontally polarized light, as can be seen in

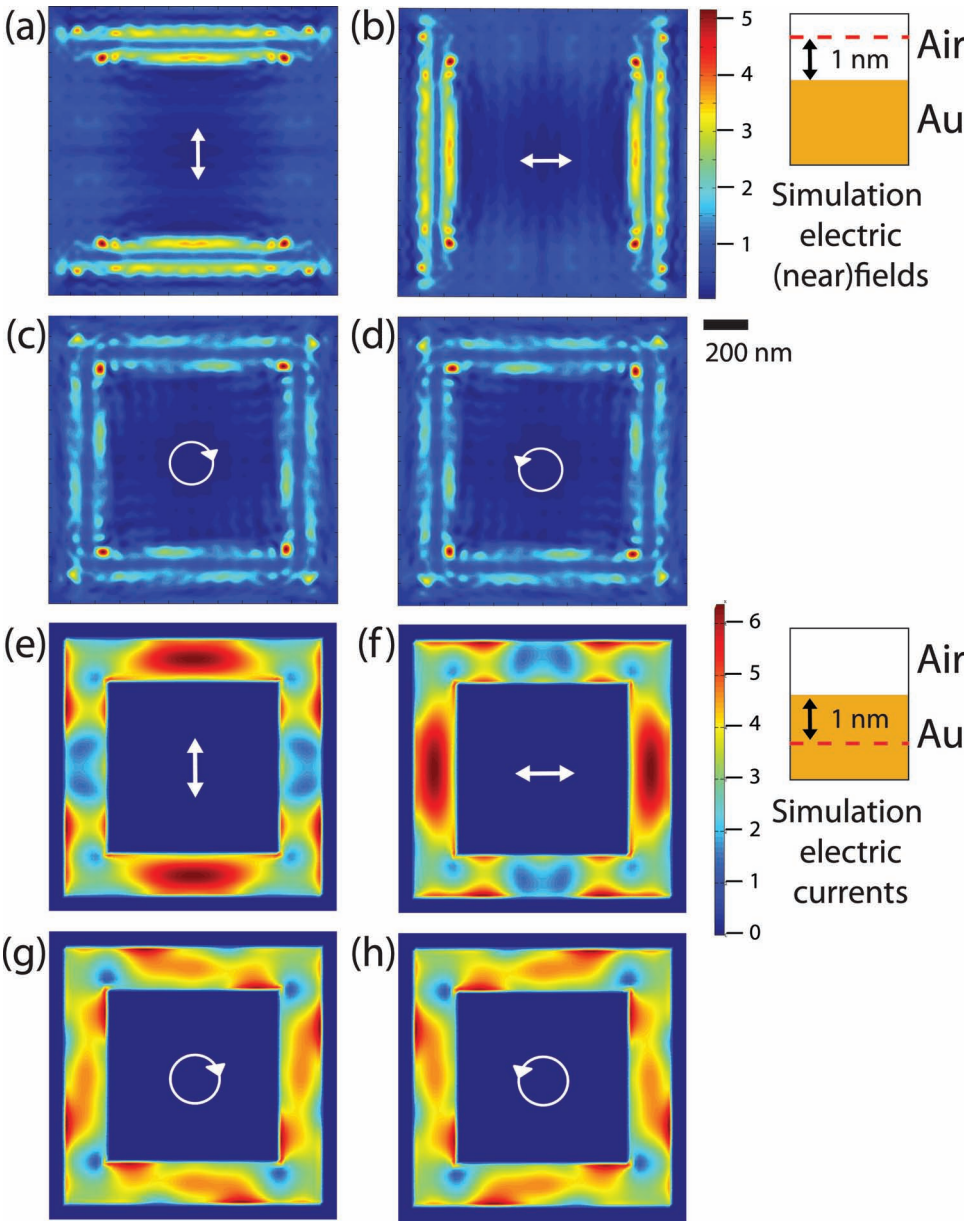

Figure 3. Numerical simulations of the electric fields and currents indicate the manner in which charges are driven in response to the polarization state of light. From (a) to (d), numerical simulations of the electric (near)fields in a plane immediately above the air/gold interface. From (e) to (h), numerical simulations of the electric currents in a plane immediately below the air/gold interface. In each case, the direction of polarization for the incident light is indicated with a white arrow or oriented circle. The color-scales are linear. The behavior associated with circularly polarized light is clearly not a direct superposition of the patterns for horizontal and vertical linearly polarized light that are shown above.

Figure 4b. It should also be noted that the paired hotspots are significantly brighter than the singles ones, which are situated at the edge of the array. This difference in intensity indicates that near-field coupling (most likely of antenna type) takes place between the nanostructures, reinforcing the near-field enhancements. These experimental observations of hotspots are in perfect agreement with the theoretical simulations for linearly polarized light. What about circularly polarized light?

Figure 4c shows a SHG micrograph from the same regions of the sample, at the same illumination intensity, but, this time, upon illumination with circularly polarized light. Contrary to the case of linearly polarized illumination, here, no hotspots can be observed. Instead, the SHG signal is rather homogeneous throughout the entire array, the observable small variations being attributable to fabrication defects of the array. Within this array, all individual square-rings are clearly distinguishable. Note that in Figure 4a and 4b, the sides of the squares on which there is no field enhancement are not distinguishable at all. Because all images in Figure 4 were obtained for the same laser power (0.4 mW), we can conclude that the reason why the entire squares are distinguishable in Figures 4c and 4d is because of a homogeneous field enhancement throughout the

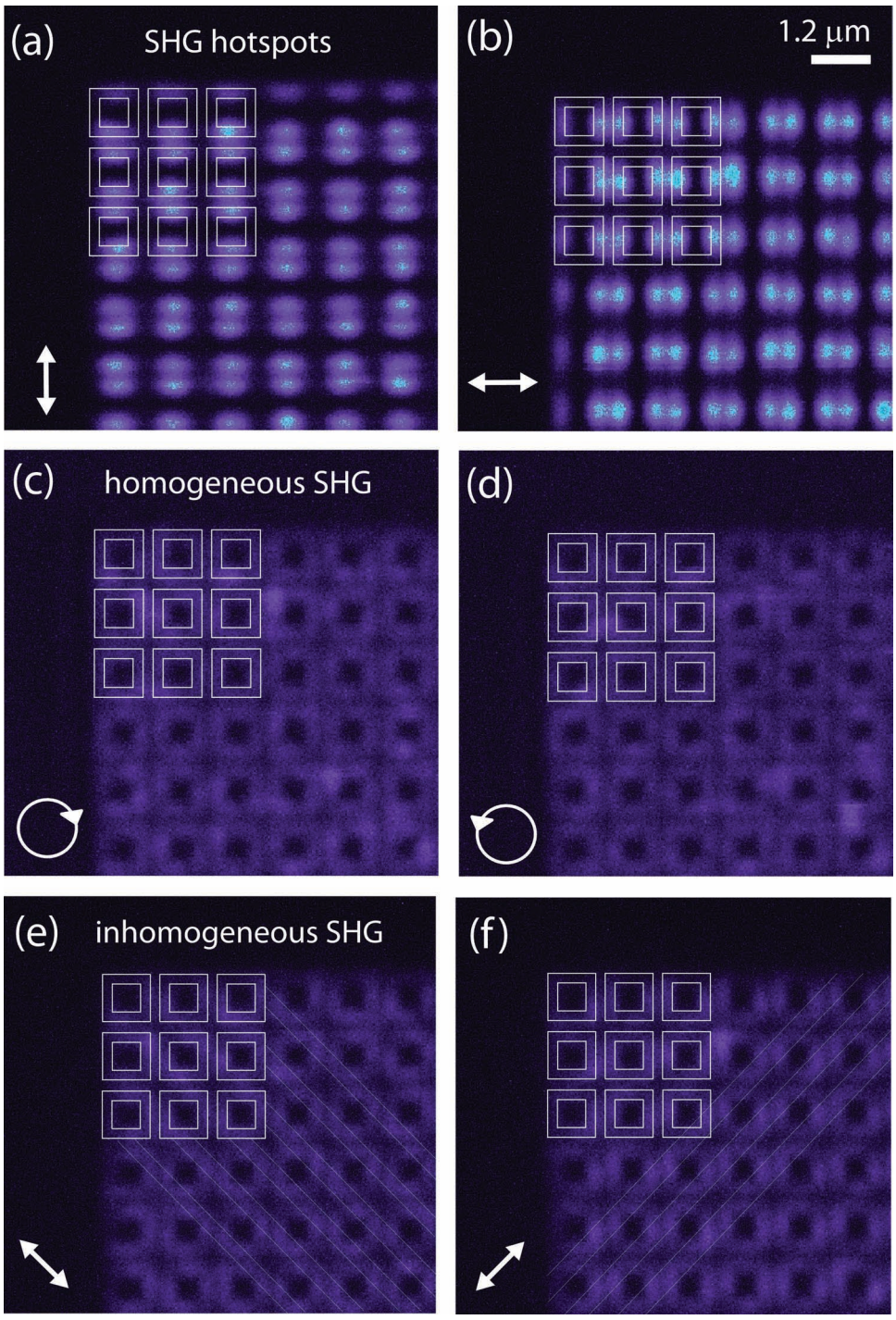

Figure 4. Second harmonic generation (SHG) matches the electric local field enhancements. In (a) and (b), SHG microscopy pictures for vertical and horizontal linearly polarized light, respectively, reveals hotspots that are mostly paired along the direction of polarization. In (c) and (d), SHG microscopy for right- and left-hand circularly polarized light shows a homogeneous SHG response from the surface of the square-rings. In (e) and (f), in response to linearly polarized incident light at + and –45°, respectively, the SHG signal is inhomogeneous. In each case, brighter and darker stripes can be observed along the direction of polarization. For clarity, the border between some of the stripes was highlighted with white lines. In all panels, the white arrows and oriented circles indicate the direction of polarization. Moreover, for clarity, the geometry of 9 nanostructures has been highlighted with white lines.

nanostructures. Moreover, in both Figures 4c and 4d, the SHG signal is weaker from the edges of the array. It follows that, upon illumination with circularly polarized light, coupling is also taking place between the nanostructures. Because these nanostructures are 200 nm apart, this cannot be a direct coupling and is more likely of antenna type. Actually, the value of 200 nm is

comparable to the resolution limit of the SHG microscope. Perhaps then the "homogeneous" SHG signal is simply a superposition of the four hotspots for vertical plus horizontal linearly polarized light, which *appears* homogeneous due to optical resolution limitations? The best way to answer this important question is to compare the results for circularly polarized light with those for randomly oriented linearly polarized light, with special attention devoted to polarization along +45° and –45°.

Figures 4e and 3d display SHG micrographs for linearly polarized light along +45° and –45°, respectively. As in the case of circularly polarized light, the nanostructures are clearly distinguishable but there is an important difference. Indeed, as it is emphasized by the white lines drawn diagonally across the nanostructured array, in the case of linearly polarized light at 45°, the SHG signal is no longer homogeneous. Figures 4a, 4b, 4e, and 4f, could create the impression that the pattern of hotspots in these nanostructures always follows the direction of linearly polarized light; in fact, this is far from being the case. For all intermediate polarization directions the pattern of hotspots appears "pinned" by the strong coupling along the Y and X directions, see the complementary information. Consequently, circularly polarized light is *necessary* in order to achieve homogeneous field enhancements. This strong experimental evidence, in combination with both sets of rigorous numerical simulations, indicate that circularly polarized light is capable of driving the electron density along ring-shaped nanostructures. Before we call this statement a proof however, there are two questions that remain to be clarified, regarding the origin of the SHG signal.

First, we have assumed that the SHG signal in Figure 4 is due to electric field enhancements, but what about the magnetic field? This is an important question because, previously, we have found that SHG originated from hotspots that corresponded to both electric and magnetic field enhancements.[14] Numerical simulations of the magnetic fields at the surface of the square-rings are shown in **Figure 5**. More specifically, Figures 5a and 5b demonstrate that, for linearly polarized

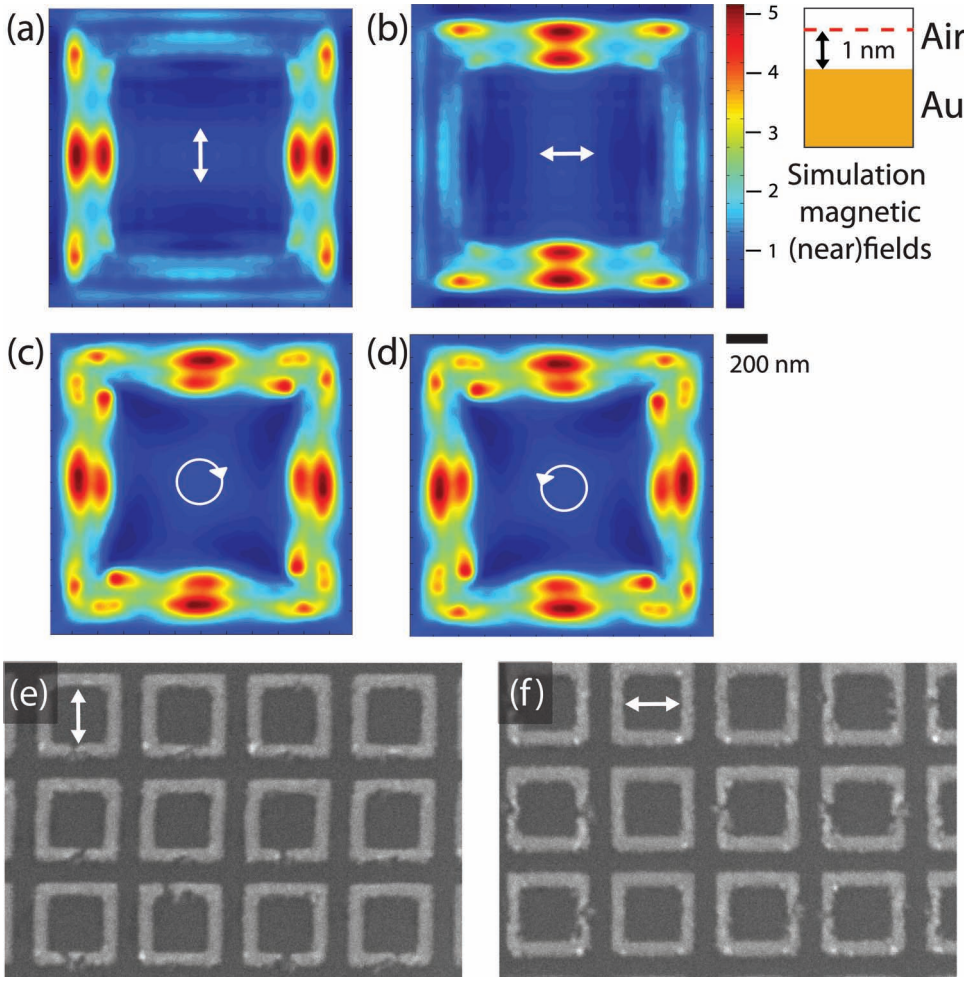

Figure 5. The locations of the magnetic near-field enhancements are clearly distinguishable from the electric ones. In (a) and (b), for vertically and horizontally linearly polarized incident light, respectively, the magnetic hotpots are situated perpendicularly to the direction of polarization. In (c) and (d), for right- and left-hand circularly polarized light, respectively, the magnetic field patterns closely resembles a superposition of the patterns associated with vertical and horizontal linearly polarized light. In (e) and (f), scanning electron microscopy of the nanostructures after illumination with laser intensity above the damage threshold. In both figures, the direction of linearly polarized light is indicated with a white arrow and the damaged regions indicate the location of highest field enhancements.

light, the magnetic field hotspots are situated on the sides of the square-rings that are *parallel* to the direction of polarization. In other words, in these particular nanostructures, electric and magnetic field enhancements are clearly distinguishable. A comparison of these fields with Figure 4a and 4b, shows unambiguously that the SHG originates from the electric and not the magnetic field enhancements. The same conclusion is reached by examining the location of the magnetic field enhancements observed in the case of circularly polarized light, see Figures 5c and 5d. Instead of a rather homogeneous field enhancements, as it is the case for electric field, these figures reveal pronounced hotspots. Such hotpots are not present in the SHG signal for circularly polarized light.

Second, in Figures 4a and 4b, the nanostructures themselves are not visible and, in order to determine the origin of the SHG hotspots, we have superimposed the layout of the nanostructured array on top of the micrographs. How unique is this superposition? In order to precisely locate the SHG hotspots, we increased the laser power to approximately 1 mW, i.e. above the damage threshold of these nanostructures. The results for vertical and horizontal linearly polarized light can be seen in Figures 5e and 5f, respectively. These figures present scanning electron microscopy images of the nanostructures, obtained after illumination. In each case, plasmon-assisted sub-wavelength laser-ablation can be observed on some of the square rings. The ablated regions correspond to the same regions, which are indicated by superposition of the layout in Figure 4a and 4b. Consequently, there can be no doubt as to how reliable these data are. Yet, sometimes, "truth is in the eye of the beholder".

Upon looking at Figure 4, it is quite obvious that the SHG signal for circularly polarized light is more uniformly distributed over the surface of the nanostructures, than the SHG signal for linearly polarized light. Why is this so obvious? To be more specific, In Figure 4, the SHG signal consists of non-zero pixels. What we mean by "uniformly distributed signal" is that these pixels are equally spaced, that there are no large gaps in between them and that there are no large variations of pixel intensity. The human eye can verify these conditions with great efficiency, however, for the purpose of better distributing the near-field on a nanostructured surface, it would be useful to be able to quantify the information.

Calculating a figure of merit for the uniformity in the near-field distribution can be done in the following manner. We begin by converting the color-scale of the SHG micrographs to grayscale, where pixel intensity is normalized to 1–white color. The black color corresponds to pixel intensity 0 and it is set at the experimental noise level. Next, for every pixel (x_i, y_j), we calculate the minimum distance to a non-zero pixel:

$$\Delta d_i = \min_{j \neq i} \sqrt{\left(x_i - x_j\right)^2 + \left(y_i - y_j\right)^2} \tag{1}$$

While in regions with uniform field distribution Δd_i is always small, in regions with large gaps within the field Δd_i is large. The average minimum distance, out of a total of N pixels, is then given by:

$$\bar{d} = \frac{1}{N} \sum_{i=1}^{N} \Delta d_i \tag{2}$$

Extensive regions of uniformly distributed near-field drive this average towards a small value. Consequently, in regions with large gaps, Δd_i deviates significantly from the average. A measure of this deviation can therefore serve as a measure of the uniformity in the near-field distribution:

$$D = \frac{1}{\bar{d}} \left(\frac{1}{N} \sum_{i=1}^{N} \left(\Delta d_i - \bar{d}\right)^2 \right)^{1/2} \tag{3}$$

where we can see that the smaller D, the more uniformly distributed the near-field is; for a perfectly uniform distribution, $\forall i$, $\Delta d_i = \bar{d}$ and $D = 0$.

Upon applying this measure to the SHG micrographs, we find that, for linearly polarized light (Figure 4b), D = 1.36. However, for circularly polarized light (Figure 4c), D = 0.68, which proves that the SHG signal is more homogeneous in the case of circularly polarized. Moreover, the variation in the pixel intensity can be evaluated upon measuring the second Pearson's skewness coefficient $\gamma = 3 \cdot (m - \mu)/\sigma$, where m is the mean, μ is the median and σ is the standard deviation. This measure on skewness evaluates the symmetry in the distribution of pixel intensities. For linearly polarized light, we find that γ = 1.12, which is a clear sign of a skewed distribution, due to the presence of hotspots. However, for circularly polarized light, we find that γ = 0.47, indicating that the distribution is more symmetric. It should be noted that the measure of homogeneity in Equation 3 is best suited for analyzing experimental results, since it relies on the noise level of the instrument in order to set the zero pixel intensity. The second Person's skewness coefficient though can be readily applied to simulation results as well. Thus, for the case of linearly polarized light in Figure 3b, γ = 0.94, while for the case of circularly polarized light in Figure 3c, γ = 0.46. These γ values are remarkably close to those obtained from the experimental results.

In conclusion, we have demonstrated that near-field enhancements can be extended over an entire nanopatterned gold surface, thereby increasing the interaction cross-section with molecules for chemical and sensing applications. The extension of the near-field is achieved by driving the electron density along loop-shaped nanostructures with circularly polarized light. The concept is validated by two sets of complementary, rigorous, numerical simulations and a clear experimental confirmation. The proof of principle presented here makes use of square-rings, which pack more efficiently than circular rings. For the purpose of obtaining more homogeneous field enhancements on a larger surface area, hexagonal rings and smaller dimensions could perhaps be investigated.

Experimental Section

Sample Preparation: Samples were prepared using a standard e-beam lithography technique. A double layer resist (PMMA/CO-PMMA) was spin coated on a Si substrate. The desired pattern is written using e-beam. The sample is then developed in MIBK/IPA mixture. This process is followed by metal deposition (3 nm Ti/30 nm Au) using sputtering. Lift-off was performed in hot acetone punctuated with mild sonication. Sample quality is then monitored with AFM and SEM.

The numerical RSoft simulations of the electromagnetic field are based on the rigorous coupled-wave analysis method, a robust algorithm that is widely used for modeling diffraction gratings and other periodic optical structures. To this end, the electromagnetic (near)-field within the periodic structure, as well as the spatial distribution of the corresponding dielectric constant, are expanded in Fourier series. Then, by using the boundary conditions at the reflection and transmission facets of the structure, one matches the incoming and transmitted fields (plane waves in our simulations) as well as the field within the structure and subsequently one computes the expansion coefficients of all the terms (harmonics) in the Fourier series. This procedure allows one to obtain an accurate description of the reflected field, transmitted field, and the optical near-field corresponding to the analyzed photonic structure. In all our numerical simulations convergence has been reached if N = 16 harmonics for each dimension have been used [this amounts to a total of $(2N+1)^2 = 1089$ harmonics].

MAGMAS models the nanostructure with 20 nm by 20 nm by 15 nm blocks. The blocks are replaced by their equivalent three dimensional electric current with known shape but unknown amplitudes. In order to obtain the unknown amplitudes, the volumetric integral equations describing the structure are subsequently solved by the Method of Moments.

SHG images are acquired with a Zeiss LSM 510 Laser Scanning Microscope (Carl Zeiss, Jena, Germany). The SHG-signal is separated from the incident light by a dichroic mirror (HFT KP650) and an additional shortpass filter (KP660). The light source is a Spectra Physics Mai-Tai Deepsee. The laser pulses are at a frequency of 80.1 MHz. The dispersion precompensation offers pulses with a FWHM width of 200 fs, at the microscope stage. For the wavelength of 800 nm, the laser power on the stage is 0.4 mW. Pixel dwell time is 102 ms and each picture is the result of 2 times averaged line scan. The incoming laser beam is focused with a 100x/1.46 objective (α Plan-Apochromat (UV) VIS IR, Carl Zeiss, Jena, Germany). In the case of linearly polarized light at 800 nm the focal spot is elliptic,[28] with $1/e^2$ waists 330 nm in the polarization direction and 440 nm in the orthogonal direction. In case of circularly polarized light at 800 nm, a round focal spot with $1/e^2$ waist 370 nm is obtained. Hence the laser fluence at 10% of the maximum power equals 5.5×10^{-3} J/cm^2.

For scanning electron microscopy, we made use of a Jeol JSM 5600. This is a standard high vacuum instrument, which uses tungsten filament as an emission source with operational voltage up to 30 kV. In our experiments, a beam of electrons is accelerated up to 20 kV before it hits the sample. The beam is raster scanned over the area of interest. At each position, the high-energy incident electrons are losing their energy via different mechanisms such as elastic, inelastic scattering, light generation, etc. In our particular setup secondary electrons are inelastically scattered from the sample, attracted by a positively biased grid and then collected by the detector. The intensity in the picture is proportional to the number of the emitted secondary electrons from the particular position. The secondary electrons have a low energy, meaning a low mean free path, so they typically originate from a region very close to the sample surface, which allows very good spatial resolution (a few nm).

Acknowledgements

We are grateful to Saloomeh Shariati from the crypto group in the Université Catholique de Louvain, for helpful discussion on the measures of the uniformity in images. We acknowledge financial support from the fund for scientific research Flanders (FWO-V), the K. U. Leuven (CREA, GOA), Methusalem Funding by the Flemish government and the Belgian Inter-University Attraction Poles IAP Programmes. V. K. V. and S. V. are grateful for the support from the FWO-Vlaanderen. B. DC. is thankful to the IWT.

Received: March 20, 2012
Published online: July 3, 2012

[1] S. A. Maier, in *Plasmonics: Fundamentals and Applications*, Springer, **2007**.
[2] T. Chen, H. Wang, G. Chen, Y. Wang, Y. Feng, W. Shan Teo, T. Wu, H. Chen, *ACS Nano* **2010**, *4*, 3087–3094.
[3] K. H. Dostert, M. Álvarez, K. Koynov, A. del Campo, H. J. Butt, M. Kreiter, *Langmuir* **2012**, *28*, 3699–3703.
[4] A. Nitzan, L. E. Brus, *J. Chem. Phys.* **1981**, *75*, 2205–2214.
[5] C. J. Chen, R. M. Osgood, *Phys. Rev. Lett.* **1983**, *50*, 1705–1708.
[6] D. L. Jeanmaire, R. P. Van Duyne, *J. Electroanal. Chem.* **1977**, *84*, 1–20.
[7] M. G. Albrecht, J. A. Creighton, *J. Am. Chem. Soc.* **1977**, *99*, 5215–5217.
[8] M. I. Stockman, *Top. Appl. Phys.* **2006**, *103*, 47.
[9] K. Kneipp, Y. Wang, H. Kneipp, L. T. Perelman, I. Itzkan, R. R. Dasari, M. S. Feld, *Phys. Rev. Lett.* **1997**, *78*, 1667.
[10] S. Nie, S. R. Emory, *Science* **1997**, *275*, 1102.
[11] V. K. Valev, A. V. Silhanek, Y. Jeyaram, D. Denkova, B. De Clercq, V. Petkov, X. Zheng, V. Volskiy, W. Gillijns, G. A. E. Vandenbosch, O. A. Aktsipetrov, M. Ameloot, V. V. Moshchalkov, T. Verbiest, *Phys. Rev. Lett.* **2011**, *106*, 226803.
[12] V. K. Valev, D. Denkova, X. Zheng, A. I. Kuznetsov, C. Reinhardt, B. N. Chichkov, G. Tsutsumanova, E. J. Osley, V. Petkov, B. De Clercq, A. V. Silhanek, Y. Jeyaram, V. Volskiy, P. A. Warburton, G. A. E. Vandenbosch, S. Russev, O. A. Aktsipetrov, M. Ameloot, V. V. Moshchalkov, T. Verbiest, *Adv. Mater.* **2011**, *24*, OP29.
[13] H. Cang, A. Labno, C. Lu, X. Yin, M. Liu, C. Gladden, Y. Liu, X. Zhang, *Nature* **2011**, *469*, 385–388.
[14] I. I. Smolyaninov, A. V. Zayats, C. C. Davis, *Phys. Rev. B* **1997**, *56*, 9290–9293.
[15] E. J. R. Vesseur, R. de Waele, M. Kuttge, A. Polman, *Nano Lett.* **2007**, *7*, 2843–2846.
[16] C. Hrelescu, T. K. Sau, A. L. Rogach, F. Jackel, G. Laurent, L. Douillard, F. Charra, *Nano Lett.* **2011**, *11*, 402–407.
[17] T. Kosako, Y. Kadoya, H. F. Hofmann, *Nat. Photonics* **2010**, *4*, 312–315.
[18] V. K. Valev, X. Zheng, C. G. Biris, A. V. Silhanek, V. Volskiy, B. De Clercq, O. A. Aktsipetrov, M. Ameloot, N. C. Panoiu, G. A. E. Vandenbosch, V. V. Moshchalkov, *Opt. Mater. Express* **2011**, *1*, 36–45.
[19] Diffract MOD, RSoft Design Group. http://www.rsoftdesign.com
[20] M. Vrancken, G. A. E. Vandenbosch, *IEEE Trans. Microwave Theory Techn.* **2003**, *51*, 216–225.
[21] Y. Schols, G. A. E. Vandenbosch, *IEEE Trans. Antennas Propagat.* **2007**, *55*, 1086–1094.
[22] V. K. Valev, N. Smisdom, A. V. Silhanek, B. De Clercq, W. Gillijns, M. Ameloot, V. V. Moshchalkov, T. Verbiest, *Nano Lett.* **2009**, *9*, 3945.
[23] J. Butet, J. Duboisset, G. Bachelier, I. Russier-Antoine, E. Benichou, C. Jonin, P.-F. Brevet, *Nano Lett.* **2010**, *10*, 1717–1721.
[24] J. Butet, G. Bachelier, J. Duboisset, F. Bertorelle, I. Russier-Antoine, C. Jonin, E. Benichou, P.-F. Brevet, *Opt. Express* **2010**, *18*, 22314–22323.
[25] V. K. Valev, A. Volodin, A. V. Silhanek, W. Gillijns, B. De Clercq, Y. Jeyaram, H. Paddubrouskaya, C. G. Biris, N. C. Panoiu, O. A. Aktsipetrov, M. Ameloot, V. V. Moshchalkov, T. Verbiest, *ACS Nano* **2011**, *5*, 91–96.
[26] M. J. Huttunen, G. Bautista, M. Decker, S. Linden, M. Wegener, M. Kauranen, *Opt. Mater. Express* **2011**, *1*, 46–56.
[27] V. K. Valev, A. V. Silhanek, B. De Clercq, W. Gillijns, Y. Jeyaram, X. Zheng, V. Volskiy, O. A. Aktsipetrov, G. A. E. Vandenbosch, M. Ameloot, V. V. Moshchalkov, T. Verbiest, *Small* **2011**, *7*, 2573–2576.
[28] R. Dorn, S. Quabis, G. Leuchs, *J. Mod. Opt.* **2003**, *50*, 1917–1926.